RSC Advances

PAPER

View Article Online
View Journal | View Issue

Cite this: *RSC Adv.*, 2017, **7**, 30919

Highly effective K-Merlinoite adsorbent for removal of Cs^+ and Sr^{2+} in aqueous solution

Yuki Kakutani,[a] Patcharaporn Weerachawanasak,[b] Yoshiya Hirata,[a] Makoto Sano,[ab] Toshimitsu Suzuki[a] and Takanori Miyake *[ab]

K-Merlinoite or "K-MER" was successfully synthesized and firstly employed as an adsorbent for the removal of Cs^+ and Sr^{2+} cations in aqueous solution by batch operation. The optimum conditions to synthesize K-MER were hydrothermal temperature of 250 °C and a hydrothermal time of 8 h. As revealed by XPS, TG, NMR, and ICP analyses, the composition of K-MER synthesized under optimum conditions was "$K_{10.9}Al_{11.2}Si_{20.9}O_{61.6}\cdot 17.8H_2O$", which corresponded with the typical formula of Merlinoite zeolite. ^{27}Al MAS NMR indicated that no octahedrally coordinated aluminum existed suggesting very high purity of K-MER. The calculated theoretical ion-exchange capacity was 4.2 mmol g^{-1}, assuming exchange of the total amount of potassium. In aqueous solution, K-MER exhibited an excellent Cs^+ (≥90%) and Sr^{2+} (≥65%) removal performance with the maximum exchange capacity of 3.08 meq. g^{-1} for Cs^+ and 2.01 meq. g^{-1} for Sr^{2+}. K-MER showed higher adsorption for Cs^+ than Sr^{2+} when performed using the same adsorption conditions. Coexisting monovalent cations, Na^+ and K^+, significantly influenced Cs^+ removal more than divalent cations, Ca^{2+} and Mg^{2+}, and they were in the order of $K^+ > Na^+ > Ca^{2+} > Mg^{2+}$. The most important factor for competitive adsorption between Cs^+ and the coexisting cation was the hydrated ionic size. Cs^+ became more difficult to adsorb when Cs^+ was interfered by a coexisting cation of close size. Although the efficiency of Cs^+ removal by K-MER decreased around 50% in artificial seawater compared with that in the aqueous solution, K-MER was a promising material for Cs^+ and Sr^{2+} removal.

Received 5th April 2017
Accepted 9th June 2017

DOI: 10.1039/c7ra03867d

rsc.li/rsc-advances

1. Introduction

In the past years, serious accidents at nuclear power plants have occurred in Pennsylvania in 1979, Chernobyl in 1986, and the latest accident in Fukushima in 2011.[1,2] Large amounts of radioactive elements, especially abundant fission products of uranium such as ^{137}Cs and ^{90}Sr were released and contaminated soil, forests, and water. Both ^{137}Cs and ^{90}Sr are very harmful to health because they are beta-gamma emitters, which have a long half-life of around 30 years.[3,4] In addition, several processes from nuclear facilities such as power plants, fuel processing, nuclear weapon testing, or remediation *etc.* generate significant volumes of radioactive elements.[5] Accumulation of these radioactive elements in plants and animals causes critical environmental and human health problems such as skin cancer and leukemia. Therefore, ^{137}Cs and ^{90}Sr should be removed as soon as possible.

Various techniques have been introduced to remove Cs^+ and Sr^{2+} in aqueous solution such as precipitation,[6] evaporation,[3] solvent extraction,[7] and adsorption *via* the ion-exchange.[8–11] Among these methods, adsorption *via* the ion-exchange is one of the most interesting techniques because it provides high efficiency and selectivity to remove radioactive elements, easy operation, low cost management, and environmental friendliness. Several effective materials have been developed and applied as the adsorbents such as clay mineral,[12] resin,[13] graphene oxide,[2] titanium dioxide,[14] silica gel,[15] sodium titanates,[16] zirconium phosphate,[10] ETS-1,[17] zeolites,[18–20] *etc.* Among these materials, zeolites are versatile inorganic materials and frequently used as the adsorbent in radioactive waste because generally zeolites contain some cations such as Na^+ and K^+ for charge-compensation, which can be easily cation-exchanged to facilitate high adsorption activity. Additionally, suitable aperture dimension of zeolites has an effect to achieve highly selective adsorption. Many researchers have reported Cs^+ and Sr^{2+} removal in aqueous solution with various types of zeolites such as Zeolite A, Faujasite X, Faujasite Y, Clinoptilolite, and Modernite.[3,4,18,21,22] However, a particular problem for Cs^+ and Sr^{2+} removal using zeolite is the impurities of zeolites or coexisting cations that simultaneously compete with Cs^+ and Sr^{2+} cation. These affected in remarkable decreasing of adsorption and ion-exchange efficiency. Similarly, the adsorption efficiency of zeolite was often reduced when applied as the adsorbent in

[a]*Graduate School of Science and Engineering, Environmental and Urban Major, Kansai University, 3-3-35 Yamate, Suita, Osaka 564-8680, Japan. E-mail: tmiyake@kansai-u.ac.jp; Fax: +81-6-6388-8869; Tel: +81-6-6368-0918*

[b]*Organization for Research and Development of Innovative Science and Technology, Kansai University, 3-3-35 Yamate, Suita, Osaka 564-8680, Japan*

seawater medium. Therefore, the highly effective adsorbents, which possess an excellent Cs^+ and Sr^{2+} removal performance with high selectivity, have been developed and continuously studied.

In the present work, highly effective K-Merlinoite zeolite (hereafter denoted as K-MER) was synthesized and firstly employed as the adsorbent for Cs^+ and Sr^{2+}. K-MER is known as a natural zeolite, which appears in K_2O–Al_2O_3–SiO_2–H_2O system. It has been investigated in wide applications such as membrane for gas separation, catalyst support, fertilizer in agriculture field, and ion-exchange material.[23–27] However, K-MER has never been reported as an adsorbent to remove Cs^+ and Sr^{2+} cations. Thus, the objective of this work is to synthesize a highly effective K-MER for Cs^+ and Sr^{2+} removal and then to focus on an evaluation of the influence of coexisting cations (Na^+, K^+, Ca^{2+}, Mg^{2+}) on the Cs^+ adsorption behavior in water medium. Moreover, Cs^+ adsorption in artificial seawater for K-MER was also evaluated.

2. Experimental

2.1 Materials

Amorphous silica (Aerosil 200 with a specific surface area of 200 $m^2\ g^{-1}$) was obtained from Evonik Japan. KOH (min. 85.0%), $Al(NO_3)_3\cdot 9H_2O$ (min. 99.9%), $CsNO_3$ (min. 90.0%), and $Sr(NO_3)_2$ (min. 98.0%) were obtained from Wako Pure Chemical Industries, Ltd. The artificial seawater whose composition is given in Table 1 was purchased from Nihon Pharmaceutical. Co. Ltd. All chemicals were analytical grade and used without further purification.

2.2 Synthesis of K-MER

K-MER adsorbents were prepared by the conventional hydrothermal method. A 2.03 g portion of SiO_2 powder was dispersed in 45 mL of 4 M KOH and was left to stir at 50 °C for 10 min. Then, 6.36 g of $Al(NO_3)_3\cdot 9H_2O$ dissolved in 45 mL of distilled water was added and the mixture was continuously stirred at 50 °C for 10 min. The resulting mixture was transferred into a Teflon autoclave and then the autoclave was immediately put in an oven at designated temperature and for a fixed time. The effect of various hydrothermal temperature and hydrothermal time as shown in Table 2 were studied to optimize the synthesis condition of K-MER. After the hydrothermal treatment, the resulting powder was washed twice with distilled water and then once with ethanol. Finally, the obtained material was dried in the oven at 70 °C overnight.

Table 1 Composition of artificial seawater

Chemical	Concentration (ppm)	wt%
NaCl	20 747	57.70
$MgCl_2\cdot 6H_2O$	9474	26.35
Na_2SO_4	3505	9.75
$CaCl_2\cdot 2H_2O$	1326	3.69
KCl	597	1.66
$NaHCO_3$	171	0.48
KBr	85	0.24
$Na_2B_4O_7\cdot 10H_2O$	34	0.09
$SrCl_2$	12	0.03
NaF	3	0.01
Others[a]	1	0.00

[a] Other chemicals: LiF, KI, $CoCl_2\cdot 6H_2O$, $AlCl_3\cdot 6H_2O$, $FeCl_3\cdot 6H_2O$, $Na_2WO_4\cdot 2H_2O$, $(NH_4)_6Mo_7O_{24}\cdot 4H_2O$, and $MnCl_2\cdot 4H_2O$.

Table 2 Synthesis conditions of K-MER adsorbents[a]

Temperature (°C)	Time (h)
150	8
200	8
250	8
250	24
250	168 (7 days)
250	336 (14 days)

[a] Component: SiO_2 33.9 mmol, $Al(NO_3)_3\cdot 9H_2O$ 16.9 mmol, KOH 180 mmol, and H_2O 45 mL.

2.3 Characterization of K-MER adsorbents

The XRD patterns of K-MER adsorbents were measured by X-ray diffractometer (Rigaku Corp.) in the range of 2θ from 5 to 70° using Cu Kα radiation with a Ni filter at 40 kV and 20 mA. The morphology of K-MER was analyzed by the scanning electron microscope (SEM, Hitachi FE-SEM S4000). The elemental analysis was performed by X-ray photoelectron spectroscopy (JPS-9000, JEOL Ltd.) using Mg Kα X-ray source. The sample was pre-evacuated under 3.8×10^{-6} Pa. The C 1s peak was taken as an internal standard at 285.0 eV. The chemical compositions were also determined by inductively coupled plasma spectroscopy (ICPS-7510, Shimadzu Corp). Briefly, 10.0 mg of sample was digested in 5 mL of hydrofluoric acid and then diluted with distilled water in 50 mL of volumetric flask. The Si/Al atomic ratio was confirmed by ^{29}Si and ^{27}Al solid-state magic-angle spinning NMR (JNM-ECA 400WB). Thermogravimetric analysis (TG) was carried out using Thermoplus TG 8120 (Rigaku Corp.).

2.4 Cs^+ and Sr^{2+} removal by the batch operation

Typically, Cs^+ or Sr^{2+} removal was performed in 100 mL Erlenmeyer flask as a batch reactor. Prior to the adsorption, various concentrations of Cs^+ (0.075–7.5 meq. L^{-1}) or Sr^{2+} (0.075–9.83 meq. L^{-1}) solutions were prepared by dissolving $CsNO_3$ or $Sr(NO_3)_2$ in distilled water. Then, the solution was adjusted its pH to 7.0 by using a small amount of 0.01 M HCl or 0.01 M NaOH solution. Briefly, 50 mg of adsorbent and 50 mL of $CsNO_3$ or $Sr(NO_3)_2$ solution was placed into the flask. The adsorption was carried out at room temperature under stirring with a magnetic bar in the flask with a stirring speed at 300 rpm for different contact times (0.5–24 h). After adsorption, the adsorbent was separated from Cs^+ or Sr^{2+} solution by centrifugation. The initial and final concentrations of Cs^+ or Sr^{2+} solutions were analyzed by atomic absorption spectrophotometer (AAS-Z-2010, Hitachi). Prior to analysis, both solutions were diluted with 0.1 wt% of KCl solution. The differences between the initial and

final concentrations could be ascribed to the amounts of Cs^+ or Sr^{2+} removed by the adsorbent. The experimental error from atomic absorption technique is ±5%.

To investigate the influence of coexisting cations on the Cs^+ removal performance, the Cs^+ solution was added with different electrolyte ions (Na^+, K^+, Ca^{2+}, Mg^{2+}). The initial concentration of Cs^+ was fixed at 0.75 meq. L^{-1} (100 ppm), and those of coexisting cations were ranged from 3.75–75.0 meq. L^{-1}. Furthermore, to evaluate the efficiency of K-MER on Cs^+ removal in seawater medium, the adsorption of Cs^+ was performed in artificial seawater with various Cs^+ concentrations at 0.075–0.75 meq. L^{-1} (10–100 ppm).

The Langmuir equation (eqn (1)) was applied to evaluate the adsorption behavior and calculate the maximum exchange capacity of the adsorbent.

$$\frac{C_e}{Q_e} = \frac{C_e}{Q_{max}} + \frac{1}{\alpha Q_{max}} \quad (1)$$

here, C_e is an equilibrium concentration of Cs^+ or Sr^{2+} (meq. L^{-1}), Q_e is the amount of Cs^+ or Sr^{2+} adsorbed per unit weight of adsorbent (meq. g^{-1}), Q_{max} is the maximum adsorption capacity (meq. g^{-1}), and α is a constant related to the free energy of adsorption ((meq. L^{-1})$^{-1}$).

The distribution coefficient (K_d) was determined by eqn (2).

$$K_d = [(C_0 - C_e)/C_e] \times \frac{V}{M} \quad (2)$$

here, K_d is a distribution coefficient of Cs^+ or Sr^{2+} (mL g^{-1} or L g^{-1}), C_0 is an initial concentration of Cs^+ or Sr^{2+} (meq. L^{-1}), C_e is an equilibrium concentration of Cs^+ or Sr^{2+} (meq. L^{-1}), V is the volume of the solution (mL), and M is the mass of adsorbent (g).

3. Results and discussion

3.1 Optimum conditions for synthesis of K-MER adsorbents

In order to investigate the optimum synthesis conditions of K-MER adsorbent by the hydrothermal method, K-MER adsorbents were prepared by changing hydrothermal temperature and hydrothermal time. Fig. 1 shows the XRD patterns of K-MER adsorbents synthesized at various hydrothermal temperatures from 150 to 250 °C for 8 h. Increasing of the hydrothermal temperature effected to gradually generate crystal form of K-MER. The broad peak of product synthesized at 150 °C showed only amorphous phase. By increasing the hydrothermal temperature to 200 °C and 250 °C, the crystal structure of K-MER could be formed. Complete formation of K-MER structure was obtained at 250 °C because it had the sharpest and highest relative intensities of XRD peaks corresponding to K-MER structure reported in ref. 28 and 29. This suggested that the hydrothermal temperature had a significant effect to structure formation of K-MER. K-MER is one of the naturally occurring zeolites and is generally known to be a crystalline form of pure K_2O–Al_2O_3–SiO_2–H_2O system. Typically, it is represented in a formula of $K_{10}Al_{10}Si_{22}O_{64}\cdot xH_2O$.[29,30]

In order to investigate the optimum hydrothermal time, the hydrothermal temperature was fixed at 250 °C and the hydrothermal time was varied. Fig. 2 shows the XRD patterns of K-MER adsorbents synthesized at 250 °C at various hydrothermal times. Longer hydrothermal times from 8 to 336 h caused gradual phase transformation from K-MER to Kalsilite. The characteristic XRD peaks of K-MER became smaller with the hydrothermal time from 8 to 24 h. Afterward, the characteristic peaks of Kalsilite was firstly observed at 168 h and then complete transformation of K-MER to Kalsilite could be achieved at 336 h. Kalsilite is one of aluminosilicate materials similar to zeolite and an ideal composition is reported as $KAlSiO_4$.[31] Although this material has some similarities to zeolites, Kalsilite is not a zeolite because Kalsilite is non-porous and the interstitial alkali-metal cations are not exchangeable under the conventional conditions.[31] This may imply that Kalsilite is not a good material for Cs^+ removal. Therefore, the optimum synthesis conditions of K-MER in this work, which afforded the highest quality without other phase

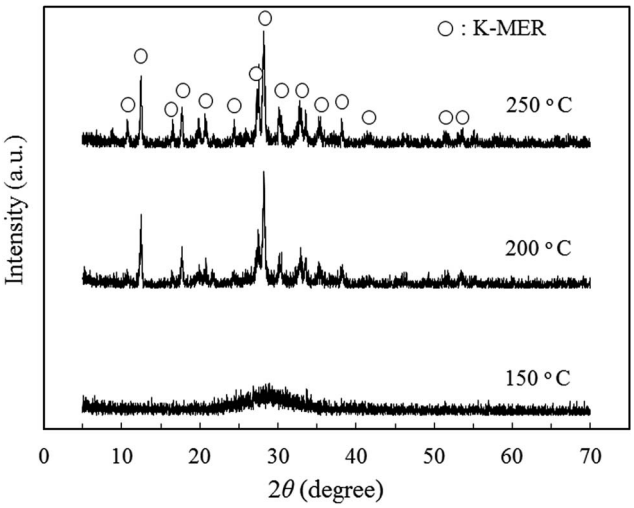

Fig. 1 XRD patterns of K-MER adsorbents hydrothermally synthesized at various temperatures for 8 h.

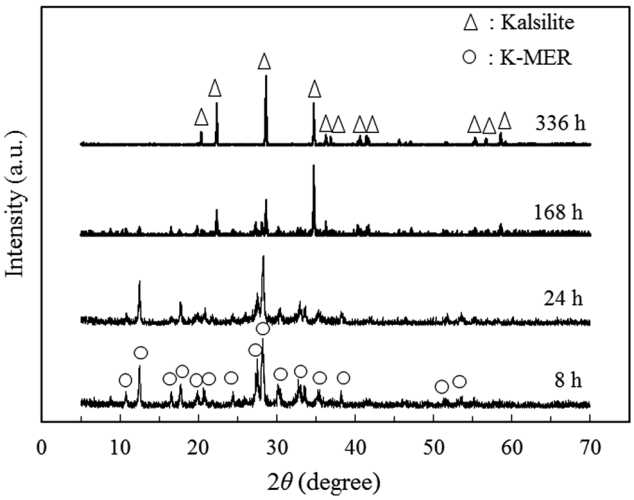

Fig. 2 XRD patterns of K-MER adsorbents hydrothermally synthesized at 250 °C at various hydrothermal times.

contamination, were hydrothermal temperature of 250 °C and hydrothermal time of 8 h.

3.2 Characterization of K-MER synthesized at optimum conditions

Hereafter, K-MER synthesized at optimum conditions (250 °C, 8 h) was analyzed by SEM, XPS, ICP, TG analysis and NMR techniques.

The morphology of K-MER was observed by SEM (Fig. 3). The morphology of K-MER showed the typical crystal habit of natural Merlionite; the bundle of tetragonal prismatic crystal shape. The crystallite size of K-MER was approximately around 0.1–0.2 μm in width with different length.[30,32]

The electronic state and chemical composition of K-MER were determined by XPS techniques. Fig. 4 illustrates the XPS spectra of (a) Si 2p, (b) Al 2p, (c) O 1s, and (d) K 2p. One symmetric peak of Si 2p at binding energy (B.E.) 103.2 eV was observed, which was assigned to Si^{4+} species in Merlinoite framework and suggesting quite energetically homogeneous environment of silicon atom. The Al 2p peak was also observed at B.E. around 74.9 eV. The peak of O 1s appeared at B.E. around 532.3 eV. Finally, the existence of K was confirmed by the two peaks of K $2p_{3/2}$ and K $2p_{1/2}$ at B.E. 294.6 and 297.3 eV,

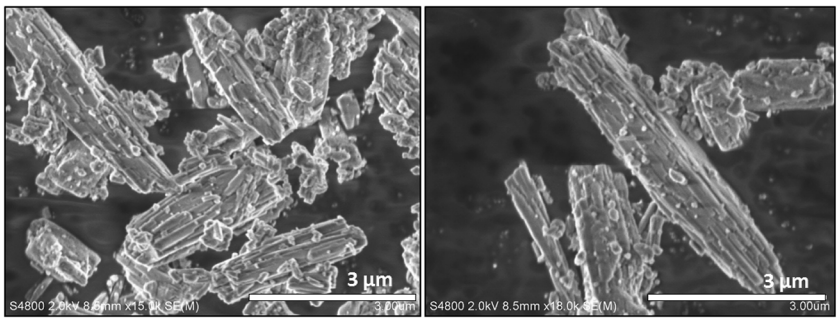

Fig. 3 SEM image of K-MER synthesized at 250 °C for 8 h.

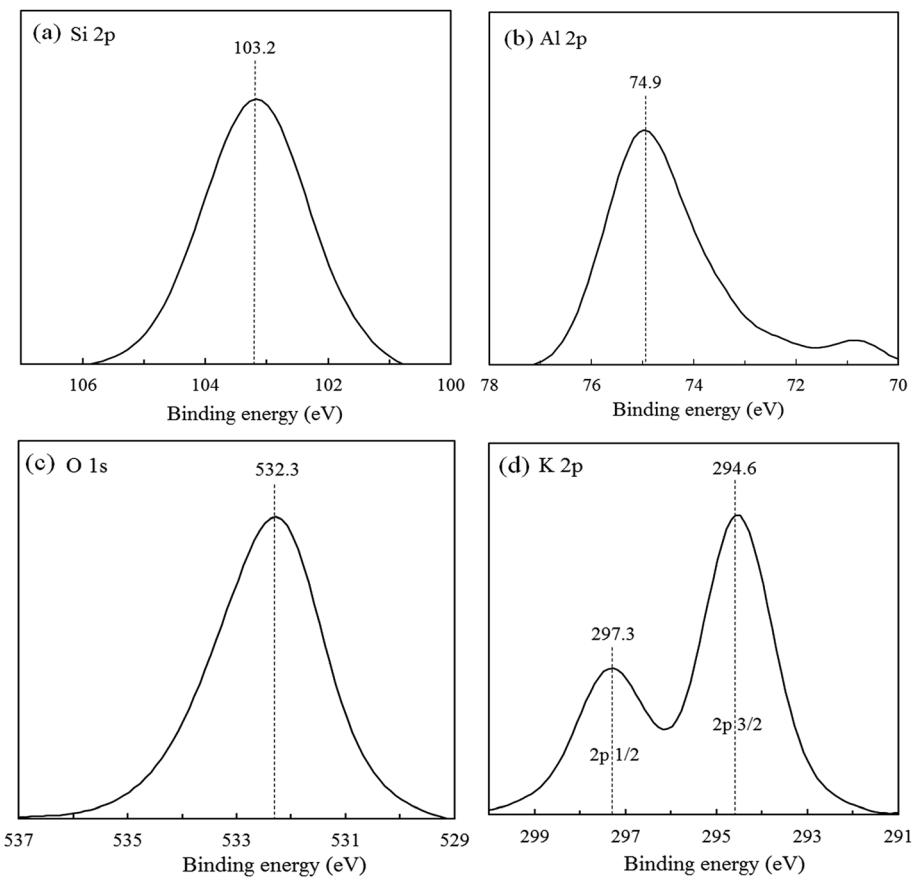

Fig. 4 XPS spectra of K-MER adsorbent. (a) Si 2p, (b) Al 2p, (c) O 1s, and (d) K 2p.

Table 3 Composition of K-MER (250 °C, 8 h) by XPS and TG analysis

Atomic composition[a] (%)						
Si	Al	O	K	Si/Al[a] [—]	H_2O[b] (wt%)	Exchange capacity[c] (mmol g^{-1})
20.0	10.7	59.0	10.4	1.87	12.3	4.2

[a] XPS analysis. [b] TG analysis. [c] Calculated by assuming total exchange of potassium.

respectively. Furthermore, the atomic composition of K-MER from XPS is summarized in Table 3. The atomic compositions of K, Al, Si, and O were calculated in the ratio of n (K) : n (Al) : n (Si) : n (O) = 10.4 (K) : 10.7 (Al) : 20.0 (Si) : 59.0 (O). It could be expressed in the composition of $K_{10.9}Al_{11.2}Si_{20.9}O_{61.6}$, which corresponds very well with the typical formula of $K_{10}Al_{10}Si_{22}O_{64}\cdot xH_2O$.[29,30] The Si/Al ratio from XPS analysis was found to be 1.87, which represents the Si/Al ratio of K-MER at near surface. However, this result was coinciding with Si/Al ratio from bulk analysis using ICP (Si/Al = 1.83). This coincidence might be because of uniform structure of synthesized K-MER.

In order to elucidate the amount of water in K-MER, TG analysis was performed from 20 to 600 °C under air flow of 180 mL-STP per min and the result is demonstrated in Fig. 5. The weight loss appeared in two steps. The first one was from 25 to 150 °C, which originated from desorption of water on the surface of K-MER. The second one was from 150 to 300 °C, which was attributed to desorption of water adsorbed in the small pore of K-MER.[33] Thereafter, no weight loss was observed from 300 to 600 °C suggesting high thermal stability of K-MER. The water contents in K-MER calculated from the total weight loss during 25 to 300 °C was 12.3%, which was equivalent to 17.8 mol of H_2O in one unit cell of K-MER. Therefore, it can be concluded that the exact molecular formula for K-MER in this work is $K_{10.9}Al_{11.2}Si_{20.9}O_{61.6}\cdot 17.8H_2O$. Additionally, the ion-exchange capacity of K-MER calculated by assuming exchange of the total amount of potassium in K-MER was found to be 4.2 mmol g^{-1}.

^{29}Si and ^{27}Al MAS NMR were measured to observe the nearest neighbor coordination environment of silicon and aluminum and to confirm purity and Si/Al ratio of K-MER. Fig. 6 shows ^{29}Si MAS NMR spectra of K-MER. There are five well deconvoluted peaks at δ −108, −103, −98, −93, and −89 ppm, which are Si(nAl) species with n = 4, 3, 2, 1, and 0, respectively, suggesting clearly five possible silicon environment.[30] Furthermore, the ^{27}Al MAS NMR spectra of K-MER (Fig. 7) showed only one symmetric peak at δ 59 ppm, which means that only tetrahedrally coordinated aluminum existed in K-MER. No octahedrally coordinated aluminum was detected around 0–25 ppm suggesting high purity of K-MER.[34,35] The Si/Al ratio calculated based on the deconvolution spectra was 1.90, which was consistent with those evaluated by XPS (Si/Al = 1.87) and ICP (Si/Al = 1.83) analyses.

From the results above, K-MER was successfully prepared by the hydrothermal method with the optimum synthesis conditions at 250 °C and for 8 h. The characteristics of K-MER in this work were in good agreement with those of Merlinoite reported by other groups.[28–30] Therefore, it can be concluded that K-MER in this work is of high purity.

3.3 Effect of synthesis conditions of K-MER on Cs^+ removal performance

The effect of synthesis conditions of K-MER such as hydrothermal temperature and hydrothermal time on Cs^+ removal

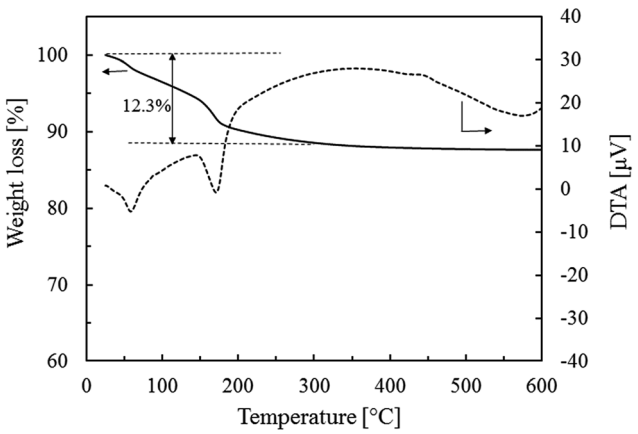

Fig. 5 Thermogravimetric and differential thermal analyses of K-MER.

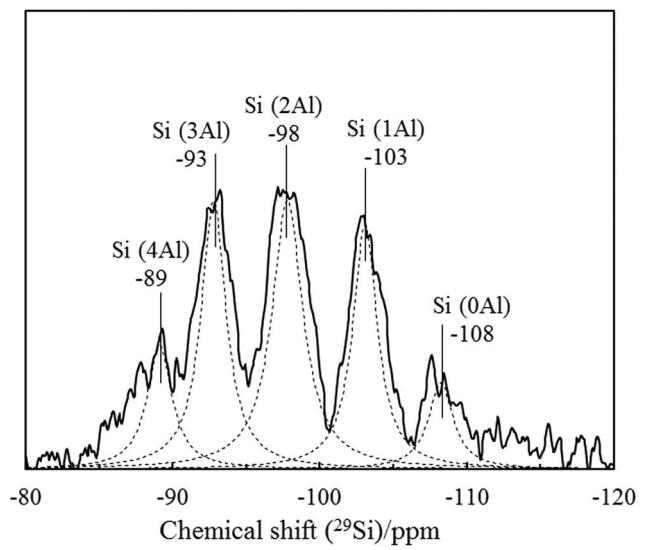

Fig. 6 ^{29}Si MAS NMR spectra of K-MER. Solid line: experimental, broken line: deconvoluted.

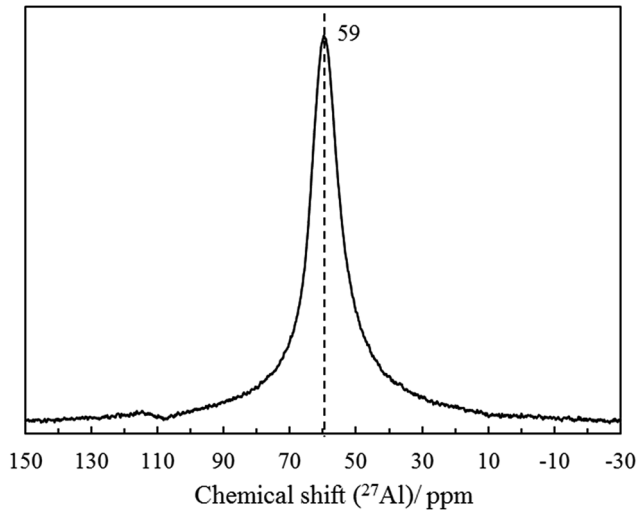

Fig. 7 ^{27}Al MAS NMR spectra of K-MER.

performance was investigated. The overall adsorption isotherms of Cs^+ removed are presented in this part.

3.3.1 Effect of hydrothermal temperature for synthesis of K-MER adsorbents on Cs^+ removal performances. K-MER adsorbents synthesized at different hydrothermal temperatures at 150, 200, and 250 °C for 8 h were tested for Cs^+ removal and results are shown in Fig. 8. Interestingly, K-MER synthesized at 200 and 250 °C showed similar excellent Cs^+ removal performances; more than 90% removal in a short time (15 min) and complete Cs^+ removal in 30 min. On the other hand, K-MER synthesized at 150 °C showed poor Cs^+ removal performance. Two key factors are generally related to high Cs^+ removal *via* the cation-exchange mechanism; (i) the high amount of cation-exchange capacity of adsorbent, and (ii) the location of available cation to be exchanged. Thus, one reason for the excellent Cs^+ removal ability of K-MER synthesized at 200 and 250 °C may be that they had more available potassium cations in high crystallinity K-MER. Meanwhile, poor Cs^+ adsorption for K-MER synthesized at 150 °C might be because of incomplete formation of crystalline structure of K-MER or amorphous material, which resulted in a low amount of exchangeable potassium in the adsorbent.

3.3.2 Effect of hydrothermal time for synthesis K-MER adsorbents on Cs^+ removal performances. Fig. 9 exhibits Cs^+ removal performances of K-MER adsorbents synthesized at 8, 24, 168, and 336 h. Both of K-MER synthesized at 8 and 24 h showed more than 95% removal within 30 min. On the other hand, K-MER synthesized at 168 h, which was composed of Merlinoite and Kalsilite, showed significantly decreased Cs^+ removal to *ca.* 75%. Obviously, no Cs removal was found on pure Kalsilite synthesized at 336 h. Thus, formation of Kalsilite at longer hydrothermal times reduced cation-exchange capacity. This is because potassium ions in Kasilite framework are interstitial cations that cannot be exchanged. Therefore, the hydrothermal time between 8 and 24 h was preferable for the high Cs^+ removal performance.

3.4 Ion-exchange capacity of K-MER for Cs^+ and Sr^{2+}

Firstly, the effect of contact time on Cs^+ and Sr^{2+} removal was investigated and the results are shown in Fig. 10. In this study, Cs^+ and Sr^{2+} removals were tested at 0.75 meq. L^{-1} at room temperature. Surprisingly, K-MER showed the excellent Cs^+ uptake of 100% in only 0.5 h. Meanwhile, for Sr^{2+} uptake, K-MER showed a moderate uptake of around 66%. The rate of Sr^{2+} ion-exchange was slow and it took 8 h to reach the equilibrium adsorption. Differences in the ion-exchange capacities and rates can be explained as follows: hydrated Sr^{2+} species have a larger size and are slow to diffuse and occupied larger space to prevent further ion-exchange.

As 24 h was sufficient to reach equilibrium adsorption, the adsorption isotherms were studied at 24 h. Fig. 11 shows the

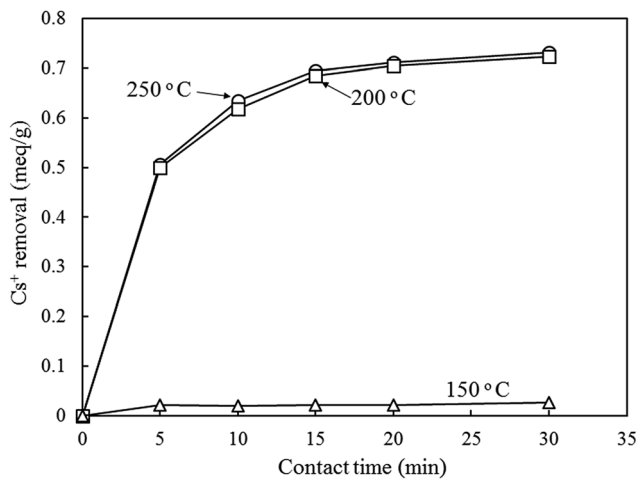

Fig. 8 Cs^+ removal performances of K-MER adsorbents hydrothermally synthesized at different hydrothermal temperatures for 8 h. Adsorption conditions: initial Cs^+ concentration 0.75 meq. L^{-1}, pH 7.0, adsorbent 0.050 g, solution 50 mL, and room temperature.

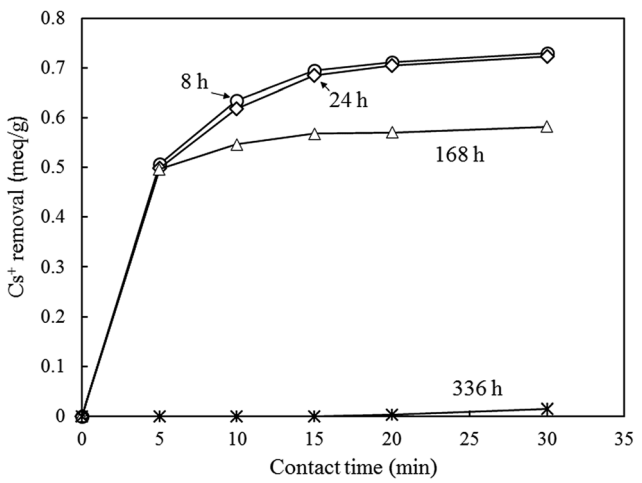

Fig. 9 Cs^+ removal performances of K-MER adsorbents hydrothermally synthesized at 250 °C at various hydrothermal times. Adsorption conditions: initial Cs^+ concentration 0.75 meq. L^{-1}, pH 7.0, adsorbent 0.050 g, solution 50 mL, and room temperature.

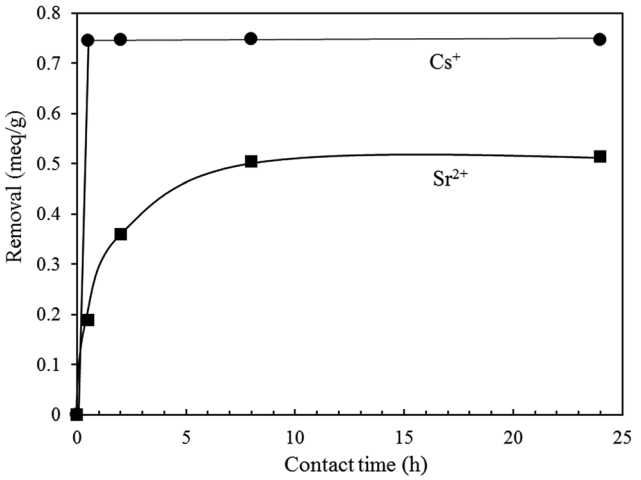

Fig. 10 Adsorption of Cs^+ and Sr^{2+} with K-MER at various contact times. Adsorption conditions: initial Cs^+ concentration 0.75 meq. L^{-1}, initial Sr^{2+} concentration 0.75 meq. L^{-1}, pH 7.0, adsorbent 0.050 g, solution 50 mL, and room temperature.

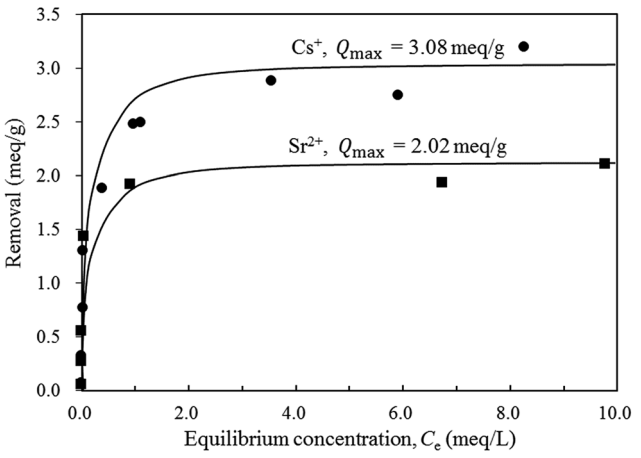

Fig. 11 Adsorption isotherms of Cs^+ and Sr^{2+} with K-MER. Adsorption conditions: initial Cs^+ concentration 0.075–7.5 meq. L^{-1}, initial Sr^{2+} concentration 0.057–5.70 meq. L^{-1}, pH 7.0, adsorbent 0.050 g, solution 50 mL, 24 h, and room temperature.

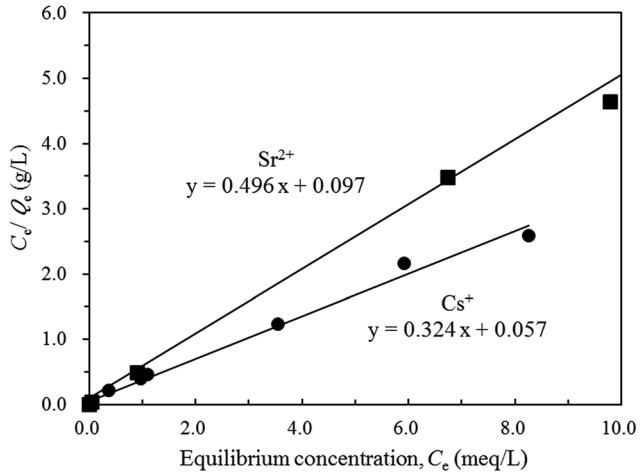

Fig. 12 Langmuir plots of Cs^+ and Sr^{2+} removal with K-MER. Adsorption conditions: initial Cs^+ concentration 0.075–7.5 meq. L^{-1}, initial Sr^{2+} concentration 0.057–5.70 meq. L^{-1}, pH 7.0, adsorbent 0.050 g, solution 50 mL, 24 h, and room temperature.

adsorption isotherms for Cs^+ and Sr^{2+}. K-MER adsorbent showed similar trends for Cs^+ and Sr^{2+} removal, but different overall performances were found. At low concentrations of Cs^+ and Sr^{2+} cations ($\leq$0.05 meq. L^{-1}), total amounts of Cs^+ and Sr^{2+} cations could be removed. When the concentration was increased from 0.05 to *ca.* 10 meq. L^{-1}, Cs^+ and Sr^{2+} removals were significantly different. It was observed that K-MER exhibited higher Cs^+ removal than Sr^{2+} removal, and the highest Cs^+ and Sr^{2+} uptakes were around 3.1 meq. g^{-1} and 2.0 meq. g^{-1}, respectively.

In order to estimate the maximum amounts of Cs^+ and Sr^{2+} removal (Q_{max}) for K-MER, the Langmuir equation (eqn (1)) was employed and the Langmuir plots for Cs^+ and Sr^{2+} removals are illustrated in Fig. 12. All the experimental data fit very well with the Langmuir adsorption model. The maximum amounts of Cs^+ and Sr^{2+} removal could be obtained from the reciprocals of the relevant slopes and they were 3.08 and 2.02 meq. g^{-1} for Cs^+ and Sr^{2+}, respectively. The lower exchange capacity of Cs^+ and Sr^{2+} for K-MER than the theoretical value, 4.2 meq. g^{-1}, might be because some potassium in K-MER framework were difficult to be exchanged. Many groups have discussed and reported the crystal structure of Merlinoite including the potassium position. Belhekar *et al.*[28] have reported that Merlinoite has two-dimensional pore structure with eight-membered oxygen rings (8MR) 5.1 × 3.4 and 3.1 × 3.5 Å. There are two types of cations sites: one surrounded by two 8MRs and the other in the larger cavity located in the niche in the double crankshaft. Further details of Merlinoite structure were revealed by Barrett *et al.*[33] Merlinoite topology is comprised of an interconnected set of 8MR channels in different dimensions, ([100] 3.1 × 3.5 Å, [010] 2.7 × 3.6 Å, [001] 3.4 × 5.1 Å + 3.3 × 3.3 Å), and potassium occupies two kinds of sites. Skofteland *et al.*[29] pronounced Merlionite structure more clearly as follows: Merlinoite has two types of 8MRs; the flat double 8MRs and the buckled 8MRs. The buckled 8MRs form the four windows into the Merlionite cage. In the hydrated Merlinoite, two potassium sites are mentioned; one is in the double 8MRs and the other one is in the Merlinoite cage. Therefore, considering two kinds of potassium sites, K^+ in the double 8MRs are more difficult to be exchanged because K^+ is surrounded by the double 8MRs. If K^+ in this site remains, then roughly two K^+ in the unit cell cannot be exchanged. This is in good agreement with *ca.* 3 mmol g^{-1} of exchange capacity against *ca.* 4 mmol g^{-1} of total exchange of K^+.

3.5 Selective adsorption of Cs^+ and Sr^{2+} cations

As indicated above, higher adsorption was found on Cs^+ rather than Sr^{2+} (Fig. 10). Many literatures stated that the adsorption selectivity sequence depended on the ionic and hydrated ionic radius of cation.[36–38] The ionic radii of K^+, Cs^+, and Sr^{2+} are 1.38, 1.67, and 1.18 Å, respectively. If the cation size is compared, Sr^{2+} is smaller and closer to K^+ than Cs^+, and therefore Sr^{2+} should

be easier to exchange with K^+ rather than Cs^+ and should provide higher Sr^{2+} uptake. However, the results did not agree with this idea. One of other important factors is the influence of hydrated ionic radii. Hydrated ionic radii of alkali and alkaline earth metals, which have strong correlation with the number of coordinated water, temperature, and rate to form hydrated shell, have been reported as follows; K^+ 2.65–2.97 Å, Cs^+ 2.95–3.21 Å, and Sr^{2+} 2.60–4.78 Å.[39,40] Hydrated radii of Cs^+ and Sr^{2+} are similar in size compared with that of K^+. However, hydration shell of Sr^{2+} is flexible in nature with a fast ligand exchange rate between the first and second hydration shell. Thus, a large hydrated Sr^{2+} radius around *ca.* 4.78 Å is reported and this may be related to low Sr^{2+} adsorption.

The distribution coefficient (K_d) was calculated by eqn (2) to confirm the adsorption selectivity of Cs^+ and Sr^{2+}. The K_d value is the ratio of metal ions adsorbed in meq. g^{-1} to metal ions remaining in the solution in meq. L^{-1}, and therefore it could be a crucial indicator to determine the selectivity of Cs^+ and Sr^{2+} adsorption. The K_d values for Cs^+ and Sr^{2+} of K-MER were 84.9 L g^{-1} and 2.2 L g^{-1}, respectively. This large difference in K_d values explains that K-MER was more selective to Cs^+ than Sr^{2+} and provided the excellent Cs^+ uptake.

3.6 Influence of coexisting cations on Cs^+ removal performance of K-MER

To evaluate the influence of coexisting cations on the Cs^+ adsorption behavior, Cs^+ adsorption was determined in the presence of Na^+, K^+, Mg^{2+}, or Ca^{2+} which were four major cations dissolved in seawater. The initial Cs^+ concentration was fixed at 0.75 meq. L^{-1} (100 ppm) whereas concentration of each cation was in the range of 5–100 times of Cs^+. Fig. 13 exhibits the influence of Na^+, K^+, Ca^{2+}, and Mg^{2+} on the Cs^+ removal performance of K-MER adsorbent. At low equivalent ratio (M/Cs = 5), K-MER kept high ability to remove Cs^+ more than 85% for all coexisting cations. Increasing of M/Cs equivalent ratio from 10 to 100 times influenced Cs^+ adsorption efficiency. The presence of Mg^{2+} cation slightly affected Cs^+ adsorption efficiency with less than 10% reduction. Ca^{2+} affected to reduce around 20% of Cs^+ adsorbed. On the other hand, the presence of Na^+ and K^+ strongly decreased Cs^+ adsorption efficiency by around 33% and 56%, respectively. It should be noted that monovalent cation (Na^+, K^+) had strongly influenced to reduce Cs^+ adsorption efficiency more than divalent cation (Ca^{2+}, Mg^{2+}). These results might be due to the difference in hydrated ionic sizes; $Na(H_2O)_6^+$ 2.4 Å, $K(H_2O)_7^+$ 2.8 Å, $Cs(H_2O)_8^+$ 3.1 Å, $Ca(H_2O)_4^{2+}$ 3.5 Å, and $Mg(H_2O)_6^{2+}$ 4.0 Å. Smaller than and closer to K^+ is easier to exchange. As the order of hydrated ionic size for four cations is $Mg^{2+} > Ca^{2+} > Cs^+ > K^+ > Na^+$, therefore K^+ in K-MER could be easily exchanged with similar hydrated cation, namely K^+, Cs^+ and Na^+. Thus, the presence of Na^+ and K^+ has significantly influenced on removal performance when the equivalent ratio of M/Cs was more than 10. On the other hand, less influence was found with coexisting Ca^{2+} and Mg^{2+} cations.

3.7 Cs^+ removal in artificial seawater

K-MER was applied to remove Cs^+ in artificial seawater that contained a large amount of matrix ions as given in Table 1. The major cations in artificial seawater were Na^+ (68.0 wt% as NaCl, Na_2SO_4, $NaHCO_3$, $Na_2B_4O_7 \cdot 10H_2O$, and NaF), Mg^{2+} (26.4 wt% as $MgCl_2 \cdot 6H_2O$), Ca^{2+} (3.7 wt% as $CaCl_2 \cdot 2H_2O$), and K^+ (1.9 wt% as KCl and KBr). At first, in order to clearly observe Cs^+ adsorption behavior of K-MER in artificial seawater, Cs^+ removal was tested at different contact times (5–30 min), at room temperature and with initial Cs^+ concentration of 0.75 meq. L^{-1}. As shown in Fig. 14, Cs^+ removal reached an equilibrium in 15 min in both distilled water and artificial seawater. At equilibrium, the maximum Cs^+ removed were 89% and 51% for distilled water and artificial seawater, respectively. Although the Cs^+ removal performance for K-MER in artificial seawater was significantly reduced compared with that in distilled water, it could be

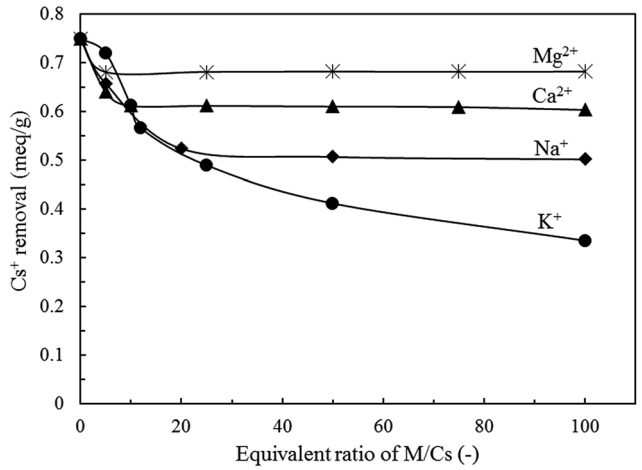

Fig. 13 Influence of coexisting Na^+, K^+, Ca^{2+}, and Mg^{2+} on the Cs^+ removal performance of K-MER. Adsorption conditions: initial Cs^+ concentration 0.75 meq. L^{-1}, M/Cs ratio = 5–100 (M: Na^+, K^+, Ca^{2+}, Mg^{2+}), solution 50 mL, pH 7.0, adsorbent 0.050 g, 24 h, and room temperature.

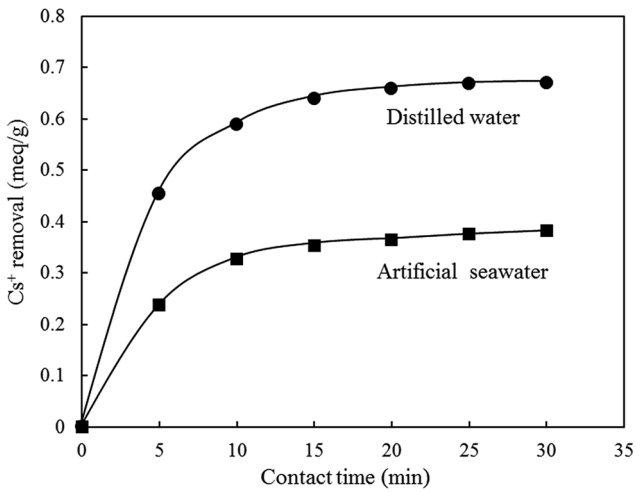

Fig. 14 Adsorption of Cs^+ in artificial seawater with K-MER. Adsorption conditions: initial Cs^+ concentration 0.75 meq. L^{-1}, solution 50 mL, pH 7.0, adsorbent 0.050 g, and room temperature.

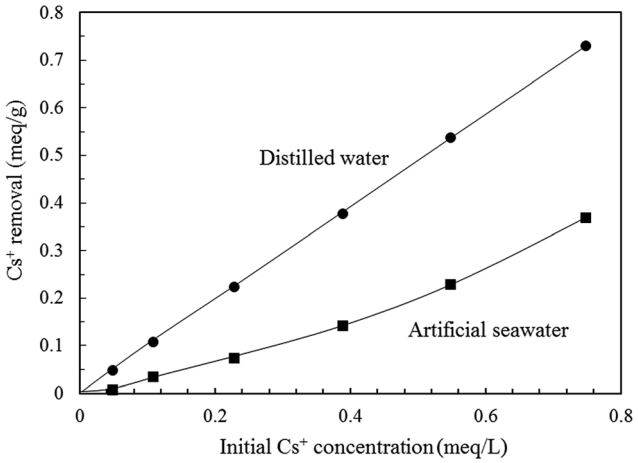

Fig. 15 Influence of initial Cs^+ concentration on adsorption of Cs^+ in artificial seawater. Adsorption conditions: initial Cs^+ concentration 0.05–0.75 meq. L^{-1}, solution 50 mL, pH 7.0, adsorbent 0.050 g, and room temperature.

remarked that K-MER is still one of the promising adsorbents because it possesses more than 50% removal in seawater. Fig. 15 shows the adsorption of Cs^+ in artificial seawater and in distilled water. Cs^+ removal in both media dramatically increased when Cs^+ concentrations were increased. Cs^+ uptakes in distilled water attained about 92–97% in every Cs^+ concentration. On the other hand, Cs^+ uptakes in artificial seawater medium varied from 10–49% depending on Cs^+ concentration; lower removal at high Cs^+ concentration.

3.8 The characteristic of K-MER adsorbent after adsorption of Cs^+

In order to clarify the Cs^+ adsorption on K-MER, the structure of K-MER after Cs^+ adsorption was investigated by XRD analysis. In addition, the reverse exchange of Cs^+ to K^+ was performed to understand if the K-MER structure is preserved. Fig. 16 shows XRD patterns of (a) K-MER (250 °C, 8 h), (b) K-MER after Cs^+ adsorption, and (c) K-MER after reverse exchange of Cs^+ to K^+. According to XRD results, the crystallinity of K-MER seemed lower after Cs^+ adsorption compared with the original K-MER (250 °C, 8 h). It was indicated that reverse exchange of Cs^+ to K^+ recovered crystallinity of K-MER. This result suggested that the structure of K-MER was not destroyed during the exchange process. Thus, K-MER is one of the promising materials to remove Cs^+ in aqueous solution.

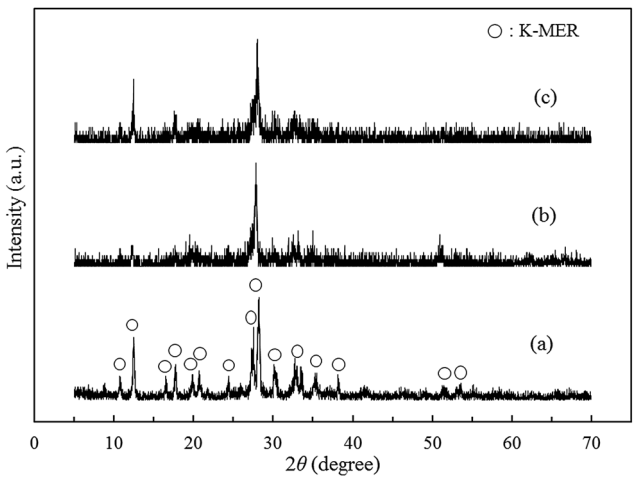

Fig. 16 XRD patterns of (a) K-MER (250 °C, 8 h), (b) K-MER after adsorption of Cs^+, and (c) K-MER after reverse adsorption of Cs^+ to K^+.

4. Conclusions

K-Merlinoite of high purity was successfully synthesized by the hydrothermal method with the optimum condition at 250 °C for 8 h. K-Merlinoite exhibited an excellent Cs^+ and Sr^{2+} removal performance with a maximum ion-exchange capacity of 3.08 meq. g^{-1} for Cs^+ and 2.01 meq. g^{-1} for Sr^{2+}. Coexisting monovalent cations significantly influenced on Cs^+ uptake while coexisting divalent cations gave a limited effect on Cs^+ removal. Moreover, K-Merlinoite showed an ability to remove Cs^+ in artificial seawater. Therefore, K-Merlinoite is an effective and promising adsorbent for Cs^+ and Sr^{2+}.

Acknowledgements

This work was partly supported by "Strategic Project to Support the Formation of Research Bases at Private Universities": Matching Fund Subsidy from MEXT (Ministry of Education, Culture, Sports, Science and Technology of Japan), 2012–2016.

Notes and references

1 B. Filipowicz, M. Pruszyński, S. Krajewski and A. Bilewicz, *J. Radioanal. Nucl. Chem.*, 2014, **301**, 889–895.
2 A. Y. Romanchuk, A. S. Kuzenkova, A. S. Slesarev, J. M. Tour and S. N. Kalmykov, *Solvent Extr. Ion Exch.*, 2016, **34**, 594–602.
3 M. W. Munthali, E. Johan, H. Aono and N. Matsue, *Journal of Asian Ceramic Societies*, 2015, **3**, 245–250.
4 D. Banerjee, U. Sandhya, S. Pahan, A. Joseph, A. Ananthanarayanan and J. G. Shah, *J. Radioanal. Nucl. Chem.*, 2017, **311**, 893–902.
5 C. Delchet, A. Tokarev, X. Dumail, G. Toquer, Y. Barre, Y. Guari, C. Guerin, J. Larionova and A. Grandjean, *RSC Adv.*, 2012, **2**, 5707–5716.
6 K. Shakir, M. Sohsah and M. Soliman, *Sep. Purif. Technol.*, 2007, **54**, 373–381.
7 E. Makrlík and P. Vaňura, *J. Radioanal. Nucl. Chem.*, 2013, **295**, 911–914.
8 A. M. El-Kamash, *J. Hazard. Mater.*, 2008, **151**, 432–445.
9 X.-H. Fang, F. Fang, C.-H. Lu and L. Zheng, *Nucl. Eng. Technol.*, 2017, **49**, 556–561.
10 A. I. Bortun, L. N. Bortun and A. Clearfield, *Solvent Extr. Ion Exch.*, 1997, **15**, 909–929.
11 S. P. Mishra, S. S. Dubey and D. Tiwari, *J. Radioanal. Nucl. Chem.*, 2004, **261**, 457–463.

12 B. Yıldız, H. N. Erten and M. Kış, *J. Radioanal. Nucl. Chem.*, 2011, **288**, 475–483.
13 S. V. S. Rao, R. Lekshmi, A. G. S. Mani and P. K. Sinha, *J. Radioanal. Nucl. Chem.*, 2010, **283**, 379–384.
14 A. Bilewicz, R. Dybczynski and J. Narbutt, *J. Radioanal. Nucl. Chem.*, 1991, **148**, 359–371.
15 K. Terada, H. Hayakawa, K. Sawada and T. Kiba, *Talanta*, 1970, **17**, 955–963.
16 N. Li, L. Zhang, Y. Chen, M. Fang, J. Zhang and H. Wang, *Adv. Funct. Mater.*, 2012, **22**, 835–841.
17 H. Liu, A. Yonezawa, K. Kumagai, M. Sano and T. Miyake, *J. Mater. Chem. A*, 2015, **3**, 1562–1568.
18 P. Rajec and K. Domianová, *J. Radioanal. Nucl. Chem.*, 2008, **275**, 503–508.
19 O. Y. Golubeva and M. V. Mokeev, *Glass Phys. Chem.*, 2016, **42**, 566–575.
20 E. H. Borai, R. Harjula, L. Malinen and A. Paajanen, *J. Hazard. Mater.*, 2009, **172**, 416–422.
21 R. O. A. Rahman, H. A. Ibrahim, M. Hanafy and N. M. A. Monem, *Chem. Eng. J.*, 2010, **157**, 100–112.
22 G. Atun and N. Bodur, *J. Radioanal. Nucl. Chem.*, 2002, **253**, 275–279.
23 J. Li, X. Zhuang, O. Font, N. Moreno, V. R. Vallejo, X. Querol and A. Tobias, *J. Hazard. Mater.*, 2014, **265**, 242–252.
24 Z. Y. Yeo, S.-P. Chai, P. W. Zhu, S.-K. Mah and A. R. Mohamed, *New J. Chem.*, 2015, **39**, 4135–4140.
25 C. Colella, D. Caputo, B. de Gennaro and E. Torracca, in *Stud Surf. Sci. Catal.*, ed. M. C. E. van Steen and L. H. Callanan, Elsevier, 2004, vol. 154, Part B, pp. 1920–1928.
26 A. Medina, P. Gamero, J. M. Almanza, A. Vargas, A. Montoya, G. Vargas and M. Izquierdo, *J. Hazard. Mater.*, 2010, **181**, 91–104.
27 P. Worathanakul, D. Trisuwan, A. Phatruk and P. Kongkachuichay, *Colloids Surf., A*, 2011, **377**, 187–194.
28 A. A. Belhekar, A. J. Chandwadkar and S. G. Hegde, *Zeolites*, 1995, **15**, 535–539.
29 B. M. Skofteland, O. H. Ellestad and K. P. Lillerud, *Microporous Mesoporous Mater.*, 2001, **43**, 61–71.
30 A. Bieniok, K. Bornholdt, U. Brendel and W. H. Baur, *J. Mater. Chem.*, 1996, **6**, 271–275.
31 J. G. Thompson, A. Melnitchenko, S. R. Palethorpe and R. L. Withers, *J. Mater. Chem.*, 1997, **7**, 673–679.
32 R. W. Tschernich, *Zeolites of the World*, Geoscience Press, 1992.
33 P. A. Barrett, S. Valencia and M. A. Camblor, *J. Mater. Chem.*, 1998, **8**, 2263–2268.
34 J. Skibsted, M. T. Pedersen and J. Holzinger, *J. Phys. Chem. C*, 2017, **121**, 4011–4017.
35 C. Wan, M. Y. Hu, N. R. Jaegers, D. Shi, H. Wang, F. Gao, Z. Qin, Y. Wang and J. Z. Hu, *J. Phys. Chem. C*, 2016, **120**, 23093–23103.
36 A. Dąbrowski, Z. Hubicki, P. Podkościelny and E. Robens, *Chemosphere*, 2004, **56**, 91–106.
37 J. T. T. Foster, Y. Hu and T. H. Boyer, *Sep. Purif. Technol.*, 2017, **175**, 229–237.
38 S. A. Abo-Farha, A. Y. Abdel-Aal, I. A. Ashour and S. E. Garamon, *J. Hazard. Mater.*, 2009, **169**, 190–194.
39 P. D'Angelo, V. Migliorati, F. Sessa, G. Mancini and I. Persson, *J. Phys. Chem. B*, 2016, **120**, 4114–4124.
40 J. Mähler and I. Persson, *Inorg. Chem.*, 2012, **51**, 425–438.